12-2018

Photocatalytic Degradation of Simazine Using ZnO/GO Composites

Kenneth Ray Flores
The University of Texas Rio Grande Valley

PHOTOCATALYTIC DEGRADATION OF SIMAZINE USING ZNO/GO COMPOSITES

A Thesis

by

KENNETH RAY FLORES

Submitted to the Graduate College of
The University of Texas Rio Grande Valley
In partial fulfillment of the requirements for the degree of

MASTER OF SCIENCE

December 2018

Major Subject: Chemistry

PHOTOCATALYTIC DEGRADATION OF SIMAZINE

USING ZNO/GO COMPOSITES

A Thesis
by
KENNETH RAY FLORES

COMMITTEE MEMBERS

Dr. Jason G. Parsons
Chair of Committee

Dr. Jose J. Gutierrez
Committee Member

Dr. Evangelina Kotsikorou
Committee Member

Dr. Arnulfo Mar
Committee Member

December 2018

ABSTRACT

Flores, Kenneth Ray, Photocatalytic Degradation of Simazine Using ZnO/GO Composites. Master of Science (MS), December, 2018, 67 pp., 6 tables, 20 figures, references, 41 titles.

The photocatalytic degradation of simazine (SIM) by Zinc oxide/graphene oxide (ZnO/GO) composites, under visible light irradiation, was investigated to determine various reaction parameters, of initial pH, ZnO loading on GO, and catalyst mass. A pH of 2 was determined to be the optimal reaction pH for all ZnO/GO catalysts. A loading mass of 40mg for the 20 & 30mmol composites; whereas a 10mg mass was determined to be most effective for the 10mmol composite. The reaction followed second order kinetics for the degradation process, the reaction dependence was determined to be on the concentration of SIM in solution. All ZnO/GO catalyst displayed a reaction rate greater than pure ZnO. Activation energies displayed a direct correlation to the amount of ZnO present on the GO surface. Further studies included catalyst cycling, which exhibited constant photocatalytic activity for the ZnO/GO composites over three reaction cycles, in addition, no priming cycle was necessary.

DEDICATION

The completion of my master studies could not have been possible without the support, love, and guidance provided by my parents, Nelda and Sigi Flores. I would also like to thank Carolina Valdes, for your actions and words continue to inspire and motivate me. Thank you all, for this accomplishment would not have not been possible without you.

ACKNOWLEDGMENTS

I would like to express my absolute gratitude to Dr. Jason Parsons, for your mentorship and guidance has catalyzed my maturation as a student, and individual. The countless hours invested into my research and academic ventures, will hardly be forgotten. A big thanks to my thesis committee members: Dr. Evangelina Kotsikorou, Dr. Jose Gutierrez, and Dr. Arnulfo Mar. Their advice, support, and guidance has encouraged me to continue my educational journey. Thank you to Helia Morales, for the constant encouragement and support you provided.

I would also like to thank my fellow lab members Daniel Ramirez, John Paul Valle, Joe Lara, Alexandria Castillo, Javier Perez, Christian Cervantes, Alexis Echevarria, and Juan Luna. The friendship and support given, by each of you, has helped me throughout countless occurrences, and for that I am grateful.

TABLE OF CONTENT

Page

LIST OF TABLES

Page

LIST OF FIGURES

Page

CHAPTER I

BACKGROUND

Characteristics of Simazine

Simazine (6-chloro-N, N'-diethyl-1,3,5-triazine-2,4-diamine, SIM) belongs to the class of chloro-s-triazine herbicides, which are primarily used for the control of broad-leaved weeds and annual grasses. SIM is a pre-emergence herbicide, meaning its application to the soil causes a disruption of root growth in germinating seedlings[1]. This compound can also be classified as a systemic herbicide, which means that once SIM molecules are absorbed they will be distributed across the plant system to susceptible tissue. The inhibition of photosynthesis, in susceptible tissues, results from a disturbance in electron transport, by interaction with SIM molecules[2]. Established non-targeted crops and plants remain unaffected by the presence of the herbicide, which makes SIM an excellent choice for a large variety of crop and non-crop usages. This herbicide is considered to be moderately persistent, lasting up to 149 days in the soil after application[3]. The inability of SIM to be absorbed by soil particles, as well as its low solubility in water (6.2 μg/ml) are factors contributing to the ability of SIM to contaminate groundwater. Ultraviolet irradiation has been well known to cause the decomposition of SIM, but this effect is minimal under normal field conditions. Microbial species are thought to be responsible for the majority of SIM decomposition in a soil medium. SIM displays a high level of stability under natural light and high temperatures, as well as in slightly acidic and basic conditions, but can be hydrolyzed by strong acids and bases[4].

History & Use

The first approved usage of simazine was in 1956 in Sweden, for use in crop and non-crop areas. It was applied over train tracks and right-of-way areas to control weed growth, as well as in crop areas including corn, asparagus, and grape root stocks. By the late 1950's simazine was being applied throughout all of Europe for the elimination of weed growth over train tracks and rights-of-way areas. By 1958 it was approved for use in the United States for crop and non-crop usage, and continued to be approved in other countries[5].

Currently simazine is used for the control of broad leave and annual grasses in crops areas such as sugarcane, corn, asparagus, nuts, citrus crops, coffee, hops, orchards, and vineyards. Before 1992 it was also used for the control of submerged weeds and algae in farm ponds, fish hatcheries, and swimming pools. The extensive use of SIM over the past sixty years, as well as its ability to permeate throughout ground water, has led to its use being controlled by State Management Programs proposed by the U.S EPA. In the United States the maximum contaminant level (MCL) for simazine in drinking water is 0.004 mg/L (0.004 ppm) or 4 ppb while the European Union has set contaminant levels to an even lower concentration of 0.1 ppb[6].

Simazine toxicity

For effects of acute toxicity, inhalation of the simazine is considered to be the most hazardous route of exposure, followed by moderate toxicity through ingestion, and a slight toxicity through dermal exposure[3]. Individuals who have an occupational exposure to SIM have reported acute dermatitis and rashes, but patch test studies on humans have concluded that sole dermal absorption does not lead to skin irritation, or sensitization[7,8]. Simazine belongs to the class of triazine herbicides, that are known to disrupt energy metabolism under acute exposure; through the disruption of thiamin and riboflavin activity. Symptoms associated with this type of

metabolism disruption include tremors, difficulty walking, convulsions, paralysis, impaired adrenal function, and diarrhea[7].

Associated symptoms of chronic SIM toxicity include damage to the testes, liver, thyroid, gene mutation, disturbance in sperm production, and tremors[7]. The EPA has set a Lifetime Health Advisory (LHA) for simazine in drinking water at 1 μg/L. Exposure to SIM, through ingestion, at or below this level should not pose a threat over the period of one's lifetime. However, ingestion well above this level, for extended periods of time, could possibly lead to the previously stated symptoms.

Environmental Fate of Simazine

The ability of simazine to leach into surface and ground water, from the soil, causes a threat to the both human and aquatic environment health. Contamination of water supplies is dependent on the sorption and desorption of SIM molecules to soil particles. The heterogenous composition of the soil, organic content, soil moisture, and influence of agricultural practices are all variables that contribute to the attraction of the herbicide molecules to the soil[8]. A comparative study testing the sorption of SIM molecules onto hydroxyl aluminum coated and uncoated montmorillonite (hydrated silicate hydroxide containing sodium, calcium, aluminum, and magnesium) particles concluded that SIM has a much stronger attraction to clay and uncoated clay surfaces at pH of 3.7[9]. Soils comprised of sand, sandy loam, and mineral rich soils had a very low adsorption of SIM molecules. The presence of organic matter (OM) in soil, appeared to increase the adsorption to simazine molecules. A study by Celis et al. found that the main bonding mechanism between OM and SIM molecules can be attributed to hydrogen bonding and proton transfer reactions between the two substances[10,11]. When taking moisture of

the soil into consideration, samples subjected to wetting and drying cycles displayed the highest values of sorption. The shrinking and swelling of the soil matrix results in a decreased surface area, which in turn permits a higher level of diffusion of SIM molecules into the soil matrix[12]. Regular tilling of farmland has been reported to reduce simazine run off. This is due to the fact that tilling enhances the number of biotic substituents present in the soil, which are responsible for the degradation of the herbicide

CHAPTER II

INTRODUCTION

Photocatalysis

A photoreaction is a chemical process driven by the absorption of light, photons, in either the ultraviolet (100 – 390nm), or visible (400-750nm) spectrum. The wavelength of light absorbed by a compound depends on its structure and more specifically the arrangement of double bonds in the compound. Upon photon absorption, electrons are promoted to the conduction band, resulting in the creation of a positively charged photo-hole (h^+) on the valence band. The promoted electron will either recombine with the photo-hole, after some form of relaxation, or create a reduced radical on the surface of the compound.

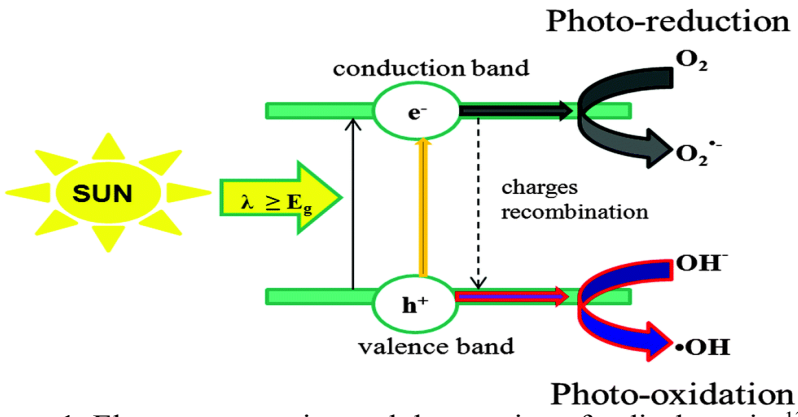

Figure 1: Electron promotion and the creation of radical species[13]

Photocatalysis refers to the acceleration of a photoreaction in the presence of catalyst, in most cases some type of semiconducting material. The photocatalytic process initiates through

photosensitization, which can occur through two separate processes. The first termed "catalyzed photoreaction" initiates with a photochemical alteration on an absorbant molecule, which then interacts with the ground state of the catalyst substrate. A "sensitized photoreaction" proceeds with initial photoexcitation, or photochemical alteration, of the catalyst, which then interacts with substrate ground state[14]. Photon absorption, and the corresponding sensitization of the photocatalyst material, drives electron promotion. This promotion brings forth a charge separation between the valance and conduction band of a compound that allows for the production of radical species. For photocatalytic driven degradation processes the formation of the hydroxyl ($OH^{\bullet}$) radical and superoxide radical ($O_2^{\bullet}$) species is crucial for the breakdown of organic compounds. These species act like an electron transport system from the semiconducting material to the organic pollutants[15].

Reactive Oxygen Species

The formation of reactive oxygen species (ROS) is a crucial step to the degradation of organic species in a photocatalytic driven process. ROS formation, extends the reach of the oxidative and reductive ability of the photocatalyst by acting like a charge transport system. Once the semiconductor material has absorbed photons, and the promotion of electrons has initiated, reductive power depends on the excited electron (e^-) in the conduction band, whereas oxidative power is generated by the newly created photo hole (h^+) in the valence band[16]. There is much debate over which (ROS) species is most crucial to the degradative processes; but it is agreed that the hydroxyl radical ($\bullet OH$) and superoxide species ($O_2^{-\bullet}$) play major roles the in the breakdown of common organic pollutants. The formation of the hydroxyl radical is thought to occur from the oxidation of water molecule by the photo hole (h^+), as well as the degradation of H_2O_2 by either interaction with light or superoxide species.

The main source of the superoxide formation occurs through the reduction of O_2 by excited electrons residing on the conduction band. The formation of ROS proceeds as followed

1. Semiconductor material (SCM) + light → SCM holes (h^+) + SCM electrons (e^-)

2. $e^- + O_2 \rightarrow O_2^{-\bullet}$

3. $h^+ + H_2O \rightarrow \bullet OH + H^+$

4. $2e^- + O_2 + 2H^+ \rightarrow H_2O_2$

5. $H_2O_2 + O_2^{-\bullet} \rightarrow \bullet OH + OH^- + O_2$

Electron spin Resonance Spectroscopy (ESR) has be performed in tandem with spin traps and spin labeling, to identify the ROS species present during degradation. For studies utilizing CdS and Ag_2S, as a photocatalyst, it was shown that superoxide (ROS) was responsible for degradation through reduction; while the photo hole served as the oxidative species towards organic matter, not the hydroxyl radical. This was determined because the corresponding energy of the photo hole was too weak to oxidize water molecules into hydroxyl radicals. These findings suggest that composition of ROS, participating in the degradative processes, depends on the band gap of the semiconducting materials. The band gap dictates the corresponding energies of the promoted electron and photo hole[17].

ZnO Structure and Properties

At room temperature (21°C) ZnO has a band gap of 3.37 eV with an associated exciton binding energy of 60 mEV. ZnO can synthesized in crystal structures of rock salt, and wurtzite; the wurtzite is the most common and displays the highest level of thermostability[18]. The hexagonal wurtzite structure has lattice parameters, a=b≠ c, of values of 0.3249nm and 0.52065 nm, at ambient pressure and temperature. This oxide is considered to be piezoelectric and pyroelectric because of its non- centrosymmetric structure, which in the hexagonal wurtzite form belongs to the P63cm space group[19].

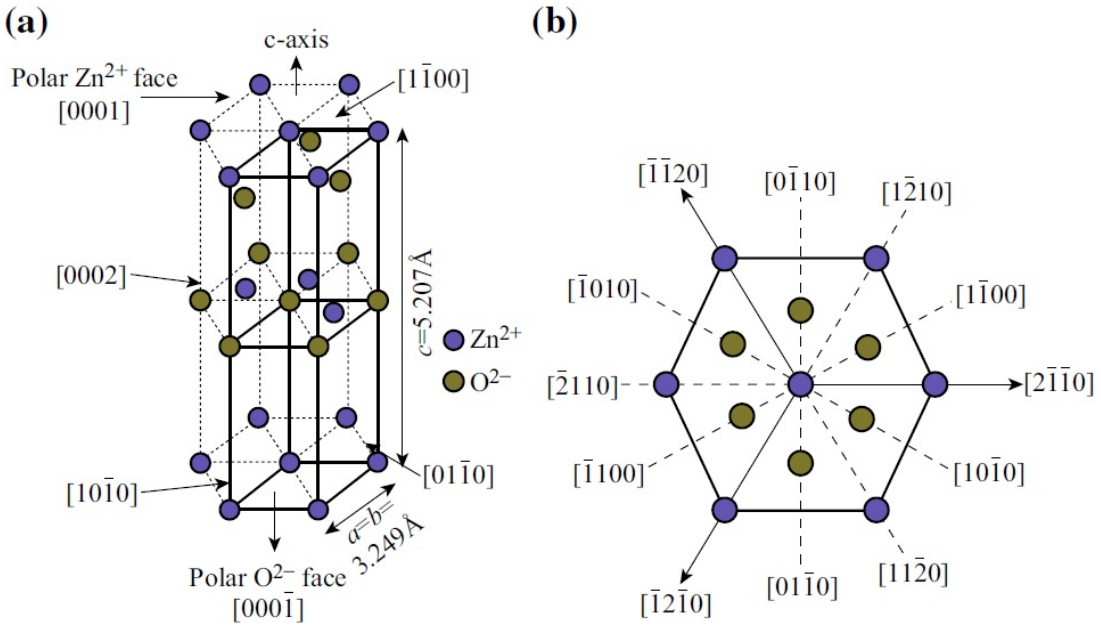

Figure 2: (a)unit cell of ZnO in the hexagonal wurtzite form (b) various crystal planes of ZnO in the hexagonal wurtzite form[20]

ZnO has been widely applied as a photocatalyst for its unique characteristics such as strong oxidation ability, direct and wide band gap, large free – exciton binding energy, and absorption in the near-UV spectral region. This oxide is considered an n-type semiconducting

material with a high level of thermostability. Considering ZnO has a similar band gap to TiO_2, it would be expected that its photocatalytic ability would be just as efficient. ZnO does pose advantages over TiO_2 with its ability to absorb a much large quanta of solar spectrum, and lower cost of production[21]. Therefor this material would be a strong candidate for large scale water treatment after optimization of its photocatalytic properties. Optimization would include circumventing issues of photocorrosion and fast recombination of photo-generated charges[22].

Graphene Oxide Structure and Properties

Many properties of graphene oxide (GO) can be tuned by chemical modification to allow for a highly specific material fabrication. GO can be doped with electron – withdrawing oxygen functionalities to create a p-type semiconductor, or modification by electron donating nitrogen groups which forms an n-type semiconductor. The band gap of GO can be tuned, from an insulating to conducting material, by increasing the number of oxidized sites located on its structure[23]. GO is considered to be zero-energy band gap semiconductor, due to the fact that its valence and conduction band touch one and other at the Dirac point. This attribute allows for a high level of conductivity and electron mobility across its carbon backbone.

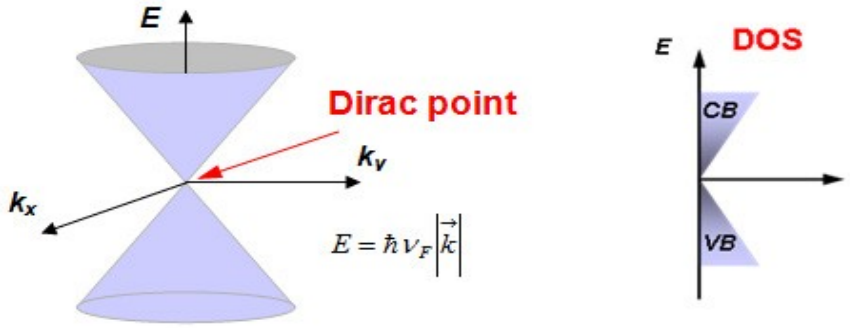

Figure 3: The Dirac point between the conduction & valence band of a Graphene Oxide[24]

The large amount of oxygen containing functional groups, on the surface of GO, allows for the anchoring of metal containing semi-conductor materials. Incorporation of the aforementioned materials could lead to a composite with characteristics of an efficient photocatalyst[25,26]. This

high level of efficiency would be attributed to GO acting as an electron transport bridge and/or electron sink for extension of carrier recombination. As well as an effective photosensitizer to the corresponding metal containing semi-conductor material, with appreciable levels of stability for long-term photocatalytic application[27].

Applications of Metal Oxide Photocatalyst

Metal oxide photocatalyst have a broad spectrum of applications including water and air purification, deodorizing, energy production and storage, solar energy devices, and self-sterilizing materials[28,29,30,31]. These reactions rely on either irradiation by UV or visible spectrum light, as a source of energy. A metal oxide photocatalyst that operates efficiently under a visible spectrum source, is desired for field application. Common metal oxide photocatalyst include TiO_2, ZnO, SnO_2, and CeO_2; these metal oxides have risen in popularity for practical applications due to their high activity, good stability, low cost, non-toxicity, and chemical inertness[32,33].

Industrialization has led to contamination over a large percent of water sources worldwide, these contaminants include pesticides, herbicides, dyes, and volatile organic molecules. Conventional water treatment is not effective to decontaminate these persistent pollutants. Therefor research and development in effective removal methods, of the aforementioned compounds, has increased in interest[34]. Heterogenous metal oxide photocatalysis has emerged as a new technology to remediation of these organic pollutants. Metal oxide photocatalyst generate reactive species, during periods of excitation, which are capable of mineralizing many dyes and herbicides. Photocatalytic material with the ability to absorb energy, in the visible spectrum of light, would be best suited for environmental remediation methods.

When photocatalytic materials are exposed to light, the contact angle with H_2O decreases, with enough excitation H_2O molecules come into even contact with the substrate forming a highly uniform thin film. The hydrophilic nature of the catalyst allows for steady stream of water across its surface, removing things such as dust particles, creating a self-cleaning product. TiO_2, employed as a photocatalyst, has the ability to degrade organic molecules when exposed to UV light. Therefor this material has been incorporated into self -cleaning TiO_2 coated surfaces. These coated material products maintain cleanliness under periods of irradiation, cutting costs and dependence on materials such as detergents. Fujishima et al. was the first to develop a self-cleaning material with titanium– coated ceramic tile[35]. Self-cleaning highway tunnel lamps were the first commercial product to employ this method of surface coating[36,37].

As the supply of petroleum continues to dwindle, the need for a sustainable source of energy continues to grow. Since the emergence of print-like manufacturing the incorporation of nanostructured solar cells, including TiO_2 and ZnO, into flexible rolls had been thought to be the future of solar cell technology. This alternative technology may surpass the efficiency of current panel model, while having a lower production cost and easier route of instillation[38]. Considering that sunlight and water are readily available resources, the implementation of metal oxide photocatalyst for water splitting continues to grow in interest. Nanostructures metal oxides such as TiO_2, ZnO, Ce/TiO_2, and CeO_2 are currently being investigated for their ability to liberate hydrogen atoms from water molecules[39]

CHAPTER III

MATERIALS AND METHODS

Synthesis of Graphene Oxide (GO)

Graphene Oxide was synthesized according to Hummers method. A volume of 69mL of H_2SO_4 was added to 3.0 g of graphite flakes and 1.5 g of $NaNO_3$ in a 500ml round bottom flask. The mixture was homogenized by magnetic stirring, and cooled to $0°C$. Once cooled, 9.0 g of $KMnO_4$ was added in small portions, to keep the reaction temperature below $20°C$. The resulting mixture was then heated to $35°C$ for 30 minutes, by water bath. The heating was followed by the addition of 138mL of 18.4 Ω H_2O, dropwise, to prevent the solution from exceeding a temperature of $60°C$. The subsequent mixture was then heated to $98°C$ and held at this temperature for 15 minutes. The reaction was then cooled to room temperature. This solution was combined with 420mL of 18.4 Ω H_2O and 3ml of 30% H_2O_2. The resulting GO particles were then collected through vacuum filtration and washed with multiple portions of H_2O and acetone. The final GO powder was dried overnight at $85°C$.

Synthesis of ZnO/GO Composite

1.0 g of GO was added to separate 500ml solutions of $Zn(NO_3)_2 \bullet 6H_2O$, at concentrations of 30, 20, 10 mmol. These solutions were then titrated using 1 M NaOH by volumes of 75, 50, and 25mL, respectively. The GO/Zn suspensions were heated to $60°C$, and held at this temperature for a period of 2 hours. The resulting ZnO/GO particles were filtered by vacuum filtration and washed with multiple portions of H_2O and acetone. The final powder was then dried overnight at $85°C$.

Characterizations

Characterization of the ZnO/GO composites were performed using x-ray diffraction (XRD), Ultraviolet – visible spectroscopy, and scanning electron microscopy (SEM) prior to degradative studies. Aliquots, taken during and subsequent to degradative studies, were analyzed by High Performance Liquid Chromatography (HPLC) for determination of Simazine (SIM) concentration remaining in solution.

XRD Analysis

XRD analysis was performed on a Bruker D2 Phaser Diffractometer. The diffractometer was fitted with a cobalt x- ray source generating emissions of 1.79 Å, and an Fe filter. Composite samples were analyzed from a scanning angle of 5-80° in 2θ, using a step size of 0.05° with a count time of 2 seconds per step. Fullprof software was utilized for diffraction pattern fittings, and all crystallographic data was obtained from literature values[40,41].

SEM Analysis

Scanning electron microscopy (SEM) images were obtained on a Zeiss EVO LS 10 scanning electron microscope. Electron micrographs were collected at working distance between 6.0 to 6.5 mm under accelerating voltages ranging from 10.75 to 20.71 KeV.

UV -VIS Spectroscopy

UV-Vis Spectroscopy analysis was performed on a Perkin Elmer Lambda 950 for all ZnO/GO composites. Measurements were recorded in % Reflectance from a nm range of 200-600.

HPLC Analysis

A Thermo Scientific Ultimate 3000 HPLC, equipped with a reverse phase C-18 column, was utilized to measure SIM concentrations during and subsequent to degradative studies. An acetonitrile/acetate (0.1M, pH6) buffer (35/65) was utilized as the mobile phase for all analysis. 10 µL injections of sample were loaded onto the column at a flow rate of 1mL per minute, at an oven temperature of $30°C$. Lamps were set to 220 & 225 nm for UV absorption analysis, with run times of 10 minutes per injection.

Degradation Studies

Degradation studies were performed in a New Brunswick Scientific Innova 44 incubator fitted with a 100W metal halide lamp, which has major emissions of 365, 406, 436, 546, 579 nm. The interaction of photocatalyst and SIM solution was performed in Pyrex beakers, using magnetic stir bars to homogenize the reaction solution. Once the reaction period of photocatalyst and SIM had elapsed, all samples were centrifuged at 3500 rpm for a duration of 10 minutes.

The photocatalyst studied for the degradation of SIM include 30, 20, 10 mmol ZnO/GO composite as well as pure ZnO. All studies were performed in triplicate for quality assurance and quality control purposes.

pH Study

The efficiency of the photocatalyst was tested over a pH range from 2 to 8. All pH adjustments were made with varying concentrations of HCl acid, and NaOH. 40mg of the photocatalyst was combined with 4mL of 25ppm SIM solution. The reaction mixture equilibrated under illumination, for a period of 1 hour at $20°C$.

Catalyst Loading study

Loading masses of 10, 20, 40, 60, and 80mg of photocatalyst were added to observe the effects of changing the amount of catalyst on the decomposition of SIM. The corresponding masses were combined with 4ml of 25ppm SIM solution, at optimal reaction pH. The solution was then allowed to react, under illumination, for a 1-hour period at a temperature of $20°C$.

Kinetics Studies

The concentration of SIM remaining in solution was monitored over a 2-hour degradation period. Conditions of optimal pH, of SIM solution, and loading mass of the photocatalyst was utilized for maximum photocatalytic efficiency. Reactions were performed using 4mL solutions of 25ppm SIM. Aliquots of 150 μL were taken at 15 minutes intervals. The inverse of [SIM] was graphed as a function of time to generate plots indicative of reaction order. Kinetic studies were varied at temperatures of 11, 20, and $30°C$ to generate an Arrhenius plot. The slope of corresponding trend line was used to solve for the activation energy of the degradation of SIM, for all photocatalytic reactions.

Concentration Variance Studies

Concentrations of 25, 12.5, and 6.25ppm of SIM solution were used to observe the effect of simazine concentration on the rate of reaction. Optimal pH and loading masses were used to maximize photocatalytic capability. A volume of 4mL of SIM solution was placed in a 10mL beaker with the photocatalyst, at its respective mass, and reacted for 1 hour under illumination. Aliquots of 150 µL were taken in 15-minute intervals. Studies were performed at 20 $°C$.

Cycling Studies

All photocatalytic material was subjected to three consecutive catalytic cycles, to determine the catalyst structural stability, and corresponding long-term catalyst efficiency. XRD analysis was performed before and after each catalytic cycle to monitor the structure changes resulting from each catalytic cycle. The ratio of catalyst to SIM solution was maintained; however, the reaction was scaled up to 1.5g of catalyst in 150ml of 25ppm herbicide solution. Reactions were performed for 1 hour under illumination at a temperature of 20 $°C$.

CHAPTER IV

PHOTOCATALYSIS RESULTS AND DISCUSSION

XRD Results

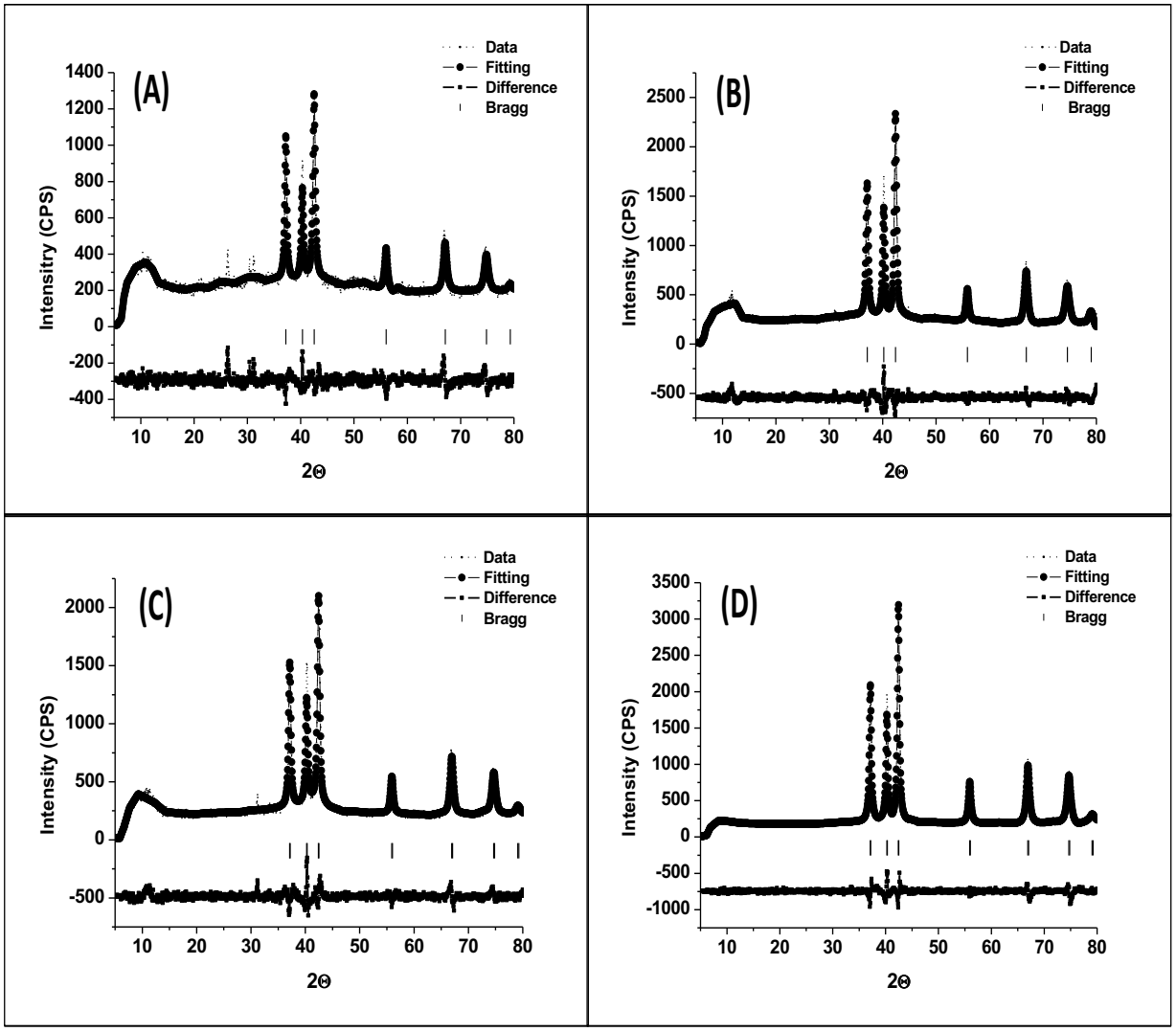

Figure 4: Diffraction patterns and fitting for (A) 10mmol ZnO/GO composite (B) 20 mmol ZnO/GO composite (C) 30 mmol ZnO/GO composite (D) pure ZnO

Sample	Phase	Space Group	a (Å)	b (Å)	c (Å)	α	β	γ	χ^2
10mmol composite	ZnO/GO	P 63 m c	3.2413	3.2143	5.1926	90	90	120	2.25
20 mmol composite	ZnO/GO	P 63 m c	3.2490	3.2490	5.2082	90	90	120	2.05
30 mmol composite	ZnO/GO	P 63 m c	3.2459	3.2459	5.2020	90	90	120	2.25
ZnO catalyst	ZnO	P 63 m c	3.246	3.246	5.2016	90	90	120	2.14

Table 1: Fitted lattice parameter for all photocatalyst

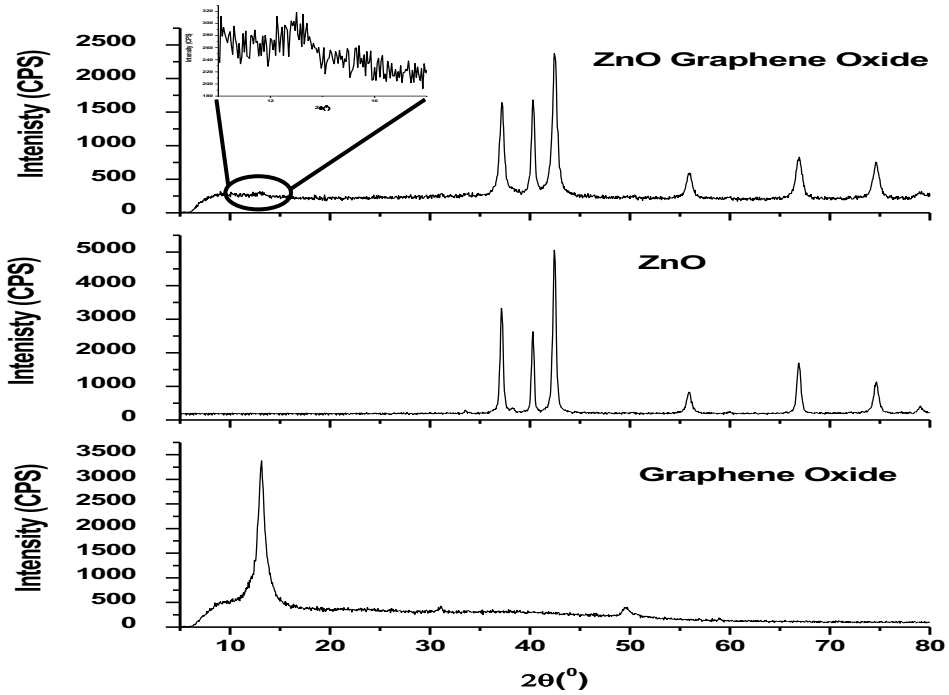

Figure 5: XRD analysis of ZnO/GO composite, ZnO, and Graphene Oxide

Phase identification, for all photocatalyst, was performed using powder X-ray diffraction. Fullprof software was utilized for the generation of X-ray diffraction fittings, by LeBail fitting procedures[42]. Crystallographic data was obtained from literature values for all photocatalyst materials[40,41].

Figure 4. displays the X-ray diffraction (XRD) patterns and fitting for the ZnO/GO (30, 20, 10mmol) and pure ZnO photocatalyst. The dotted series of lines, on the diffraction spectra, represent the raw data from the XRD analysis. The circular points, of close proximity, represents the data generated from the fittings. The series of square data points, at the bottom of the diffraction pattern represent the calculated difference between the raw XRD data and the corresponding fittings. Finally, the vertical line markings represent the corresponding Bragg lines generated from the fitting process.

Fittings for all photocatalyst has good fittings which is indicated by the χ^2 of 2.25 or lower. Considering that a $\chi^2 \leq 5.0$ is acceptable for literature submission, all generated fittings showed a good correlation between obtained and calculated values for X-ray Diffraction analysis. All of the ZnO/GO (30, 20, 10mmol) & pure ZnO photocatalyst displayed a hexagonal crystal structure, with a corresponding P 63 m c space group. In addition, the lattice parameters and angles very close to the literature with values of a = 3.2 Å, b = 3.2 Å, c = 5.2 with corresponding angels of $\alpha = 90°$, $\beta = 90°$, $\gamma = 120°$.

All four XRD spectra, for the respective catalyst, look similar distribution of the major peaks of the spectra. The pure ZnO catalyst, displayed in figure 4 D, displays 5 main peaks, three of relatively high intensity followed by two peaks of moderate to low intensity. The first major peak displayed at 37°, in 2θ, refers to the reflectance of the (100) plane of the ZnO structure, the following peak at approximately 40° refers reflectance of the (002) plane. The last peak of relative high intensity, at 42.5°, represents reflectance of the (101) plane. The two next subsequent peaks at 56° and 67° reveal reflections of the (110) and (200) planes from the ZnO structure[40]. All XRD analysis of the ZnO/GO (30, 20, 10mmol) photocatalyst displayed these characteristic peaks. There seemed to be a decrease in peak intensity, with attachment to the GO

surface; the 20 & 30mmol catalyst maintained a majority of characteristic peak intensity, while the 10mmol displayed a significant reduction of peak intensity. A low angle diffuse diffraction peak observed in all the ZnO/GO catalyst, not present in the ZnO catalyst at approximately 11° in 2θ. This is a characteristic peak of Graphene Oxide, from the (002) plane[41]. The attachment of ZnO to the GO surface brings forth a reduction of observed intensity of the aforementioned peak. Figure 5. shows the reduction of the (002) plane of GO, with a comparison of XRD analysis between GO, ZnO, and the 30 mmol ZnO/GO catalyst.

SEM Results

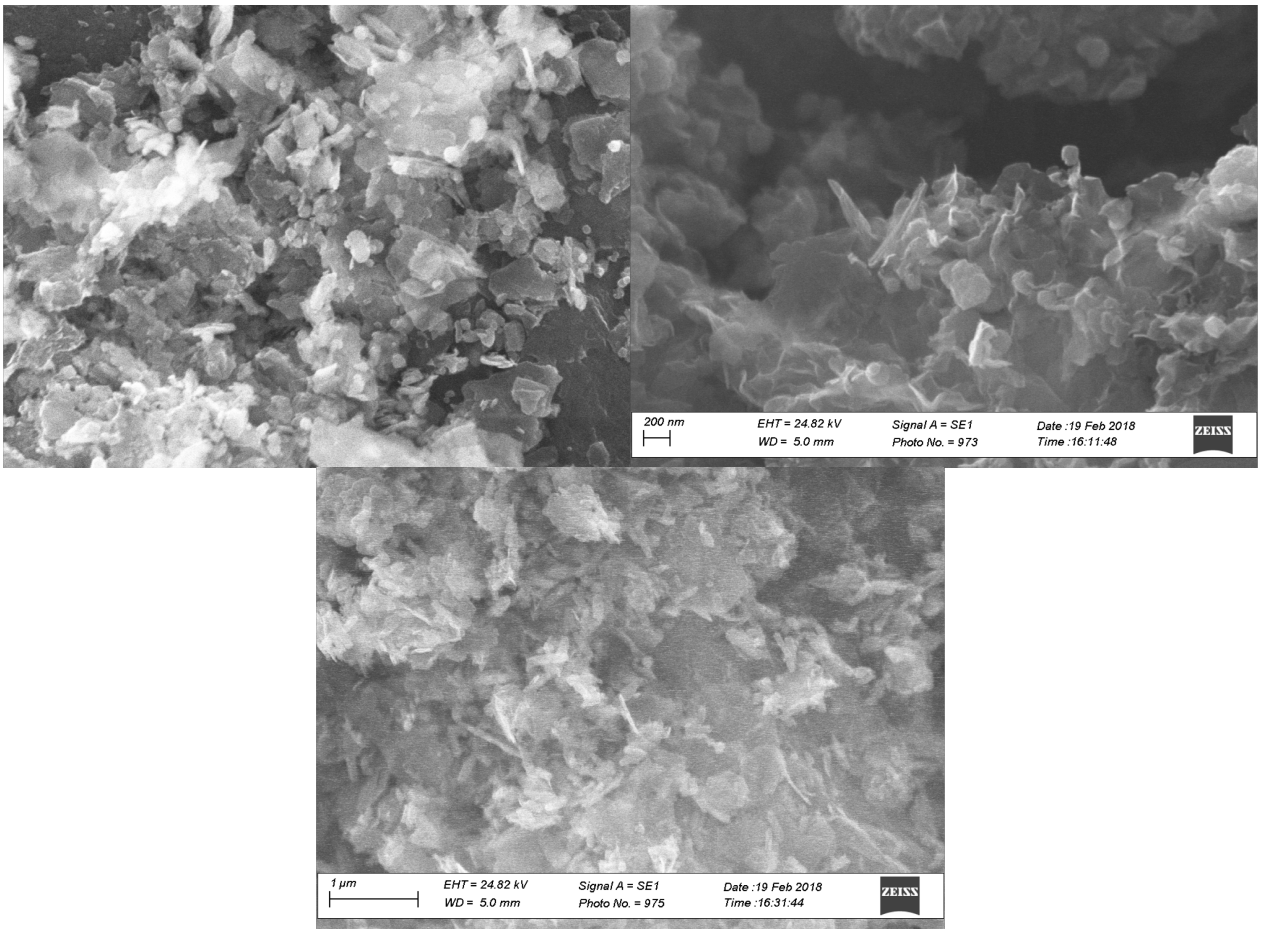

Figure 6: SEM image of 10mmol ZnO/GO composite (top left), 20mmol ZnO/GO composite (top right), 30mmol ZnO/GO composite (bottom center)

SEM images of ZnO/GO composites, displayed above in figure 6, were taken prior to any photocatalytic reactions. The top left image is of the 10mmol ZnO/GO composite, the white cluster correspond to zinc oxide platelets, attached to a graphene oxide support, the dark grey and black material. The image of the 20mmol ZnO/GO composite, top right, revealed a higher concentration of zinc oxide clusters with less exposed graphene oxide, than the image of the 10mmol material. The image of the 30mmol ZnO/GO composite, bottom center, displayed the highest concentrations of zinc oxide clusters and the least amount of exposed graphene oxide.

pH Profile Results

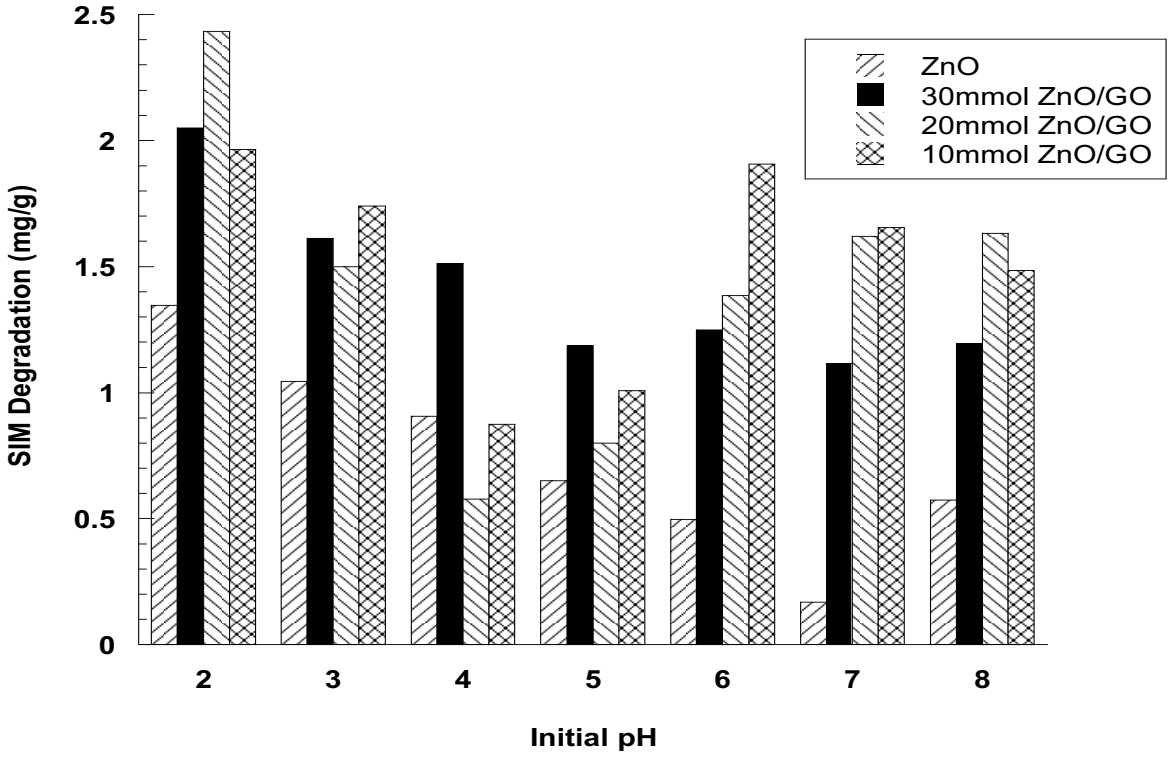

Figure 7: Effects of initial pH on the photocatalytic efficiency of ZnO/GO composites (30, 20, 10mmol) & pure ZnO

The photocatalytic efficiency of the ZnO/GO composites (30, 20, 10mmol) & pure ZnO were tested in a pH range from 2 through 8, with results displayed in Figure 7. The efficiency of the photocatalyst was based on the milligrams of SIM degraded per gram of catalyst present, during a 1-hour degradation cycle. All previously mentioned catalyst, displayed their highest catalytic activities at a pH of 2; at this pH, 2.434 mg/g of SIM was degraded by the 20mmol ZnO/GO composite, 2.049 mg/g by the 30mmol composite, 1.965 mg/g by the 10mmol composite, and 1.347 mg/g of SIM was degraded by the pure ZnO. The photocatalytic efficiency of the 20mmol composite decreased from a pH 2 to 4 (0.578 mg/g), but increased thereafter to a magnitude of 1.632 mg/g at a pH 8. The 30 mmol composite experienced a decrease in

photocatalytic efficiency, after a pH of 2, and a plateaued between a pH 5 – 8, approximately 1.2 mg/g of SIM degraded. The 10mmol composite expressed a similar trend as the 30mmol composite, with a decrease in degradation from pH 3 to 5 (0.875 mg/g), and an increased degradation thereafter to 1.485 mg/g at pH 8. Pure ZnO, showed a decrease in photocatalytic activity from pH 3 to pH 7 (0.168 mg/g), but increased at pH of 8 (0.573 mg/g).

SIM solubility decreased drastically as pH increased, by about 50% by pH 6 and thereafter; based on HPLC analysis of pH adjusted controls. A study conducted by Ward and Weber found a similar trend between pH and SIM solubility[43]. From a pH of 2 to 3, solubility decreased from 0.78 to 0.29. A solubility of 5.81 was reported for SIM at pH of 1, suggesting that neither the amino nitrogen nor hydrogen atoms were involved in the solubility mechanism. Rather the solubility is dependent on protonation of the nitrogen atoms, locked in the ring structure, at positions ortho to the chlorine substituent[43]. The kinetics of the degradation of SIM by ZnO/GO composites found that rate of the reaction depends directly on SIM concentration. The solubility of SIM coupled with reaction order indicates that a pH of 2 should be as the optimal pH for all further studies.

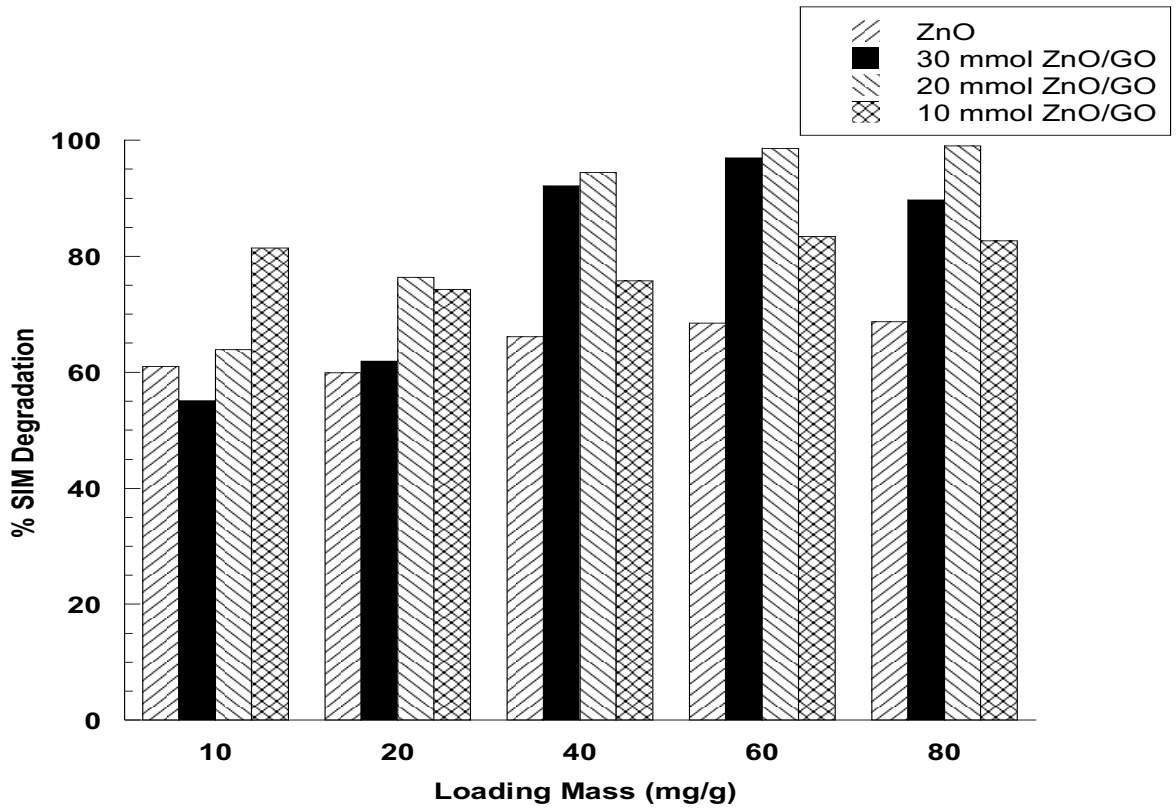

Figure 8: Effects of loading mass on the photocatalytic efficiency of ZnO/GO composites (30, 20, 10mmol) & pure ZnO

Figure 8. shows the data from the variation of loading mass of photocatalyst, ZnO/GO composites (30, 20, 10mmol) and pure ZnO, from 10, 20, 40, 60, 80mg and the correlated percent SIM degradation, during a one-hour cycle. The 20 & 30mmol ZnO/GO composites, and pure ZnO, experienced a similar trend between the correlation of loading mass to amount of SIM degraded. The variance from 10mg to 40mg brought an increase of 63.879 – 94.432% for the 20mmol composite, 55.087 – 92.121% for the 30mmol composite, and 60.991 – 68.479 for pure ZnO. From 40mg to 80mg the % of SIM degradation varied minimally; only a 4% increase was observed for the 20mmol composite, whereas a 2% increase was observed for the pure ZnO; however, a 3% decrease was observed for the 30mmol composite. The observed plateaued effect

of photocatalytic degradation, associated with higher loading masses, could be caused by increased opacity in the reaction solution[44]. With a decrease in light penetration, the ratio of SIM degradation to catalyst loading may decreases or remain constant. The 10mmol ZnO/GO composite showed a different trend between the observed % SIM degradation with variance of catalyst loading mass. Increased loading mass from 10 to 20 mg decreased % SIM degradation by 7%, from the 20 – 80mg loading mass the % of SIM degradation increased gradually to maximization at approximately 82.637%, which is approximately the same value observed for the 10mg loading sample.

Kinetic Studies Results

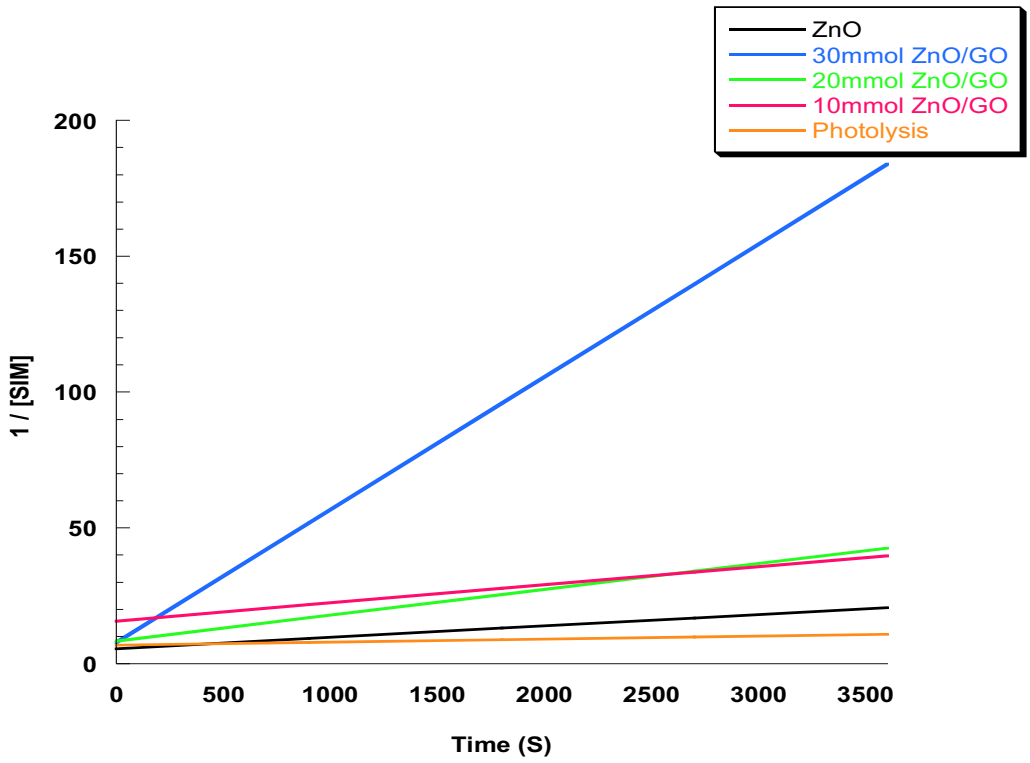

Figure 9: Kinetic plot for ZnO/GO (30, 20, 10mmol), pure ZnO, and direct photolysis 20℃

Variance in [SIM]	Instantaneous Rate
25 ppm	$4.69*10^{-3}$ mg·L^{-1}·s^{-1}
12.5 ppm	$1.45*10^{-3}$ mg·L^{-1}·s^{-1}
6.25 ppm	$3.6*10^{-4}$ mg·L^{-1}·s^{-1}

Table 2: Variance of SIM concentration & the corresponding instantaneous rates for the 30mmol ZnO/GO photocatalyst at 20℃

Variance in [ZnO]	Instantaneous Rate
30 mmol	$1.1*10^{-3}$ mg·L^{-1}·s^{-1}
20mmol	$1.3*10^{-3}$ mg·L^{-1}·s^{-1}
10 mmol	$1.3*10^{-3}$ mg·L^{-1}·s^{-1}

Table 3: 30, 20, 10 mmol ZnO variance of photocatalyst with a concentration of 25ppm of SIM at 20℃

The kinetics of the SIM degradation were determined graphically as a plot of $\frac{1}{[SIM]}$ as a function of time, with correlation coefficients of 0.99 (r^2) or better, for the photocatalytic degradation by ZnO/GO (30, 20 10mmol) and pure ZnO. The results for this study are presented in Figure 9, for all catalyst during a 1-hour reaction period. The rate constants for each reaction are equal to the slope of the individual lines expressed in L·mol^{-1}·s^{-1} The rate of degradation of SIM using the 30mmol ZnO/GO composite ($4.89*10^{-2}$ L·mol^{-1}·s^{-1}) was of the highest magnitude, followed by 20mmol composite ($9.5*10^{-3}$ L·mol^{-1}·s^{-1}), next the10mmol composite ($6.7*10^{-3}$ L·mol^{-1}·s^{-1}), followed by the pure ZnO ($4.18*10^{-3}$ L·mol^{-1}·s^{-1}), and finally direct photolysis ($1.11*10^{-3}$ L·mol^{-1}·s^{-1}). The reaction rates for all ZnO/GO composites surpass the associated rate observed for the pure ZnO catalyst; by a factor greater than 10 when compared to the rate of the 30mmol sample.

All decomposition processes of SIM by ZnO/GO composites proceeded through a 2nd order reaction. This is justified by the linear relationship, when plotting the inverse of SIM concentration remaining vs time in seconds, for all data points within a 3600 second cycle period[44]. Experimental analysis determined a 2nd order dependence on the concentration of SIM present in solution and a 0th order dependence on the concentration of ZnO present in the photocatalyst. Experimental data for this determination is presented in in tables 2 and 3.

Arrhenius Plots & Activation Energies Results

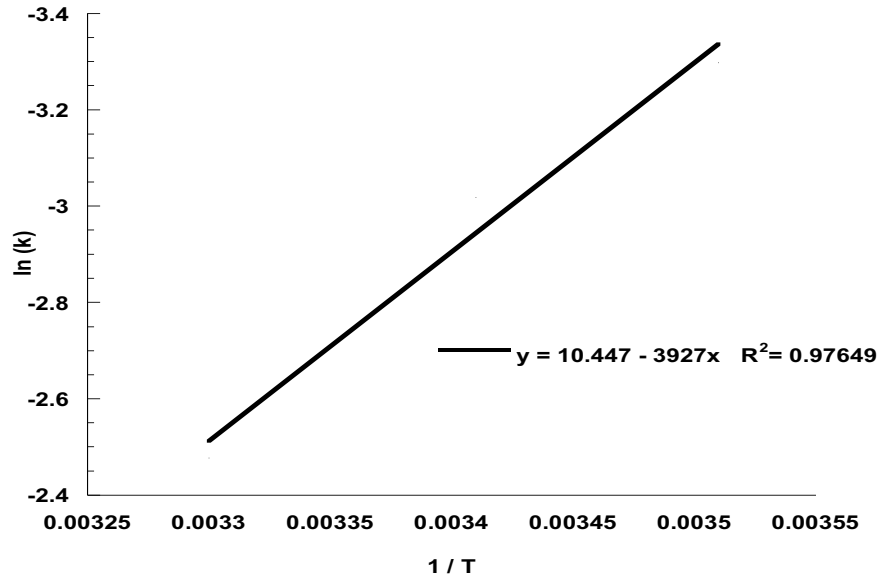

Figure 10: Arrhenius plot for the degradation of SIM by the 30 mmol ZnO/GO photocatalyst

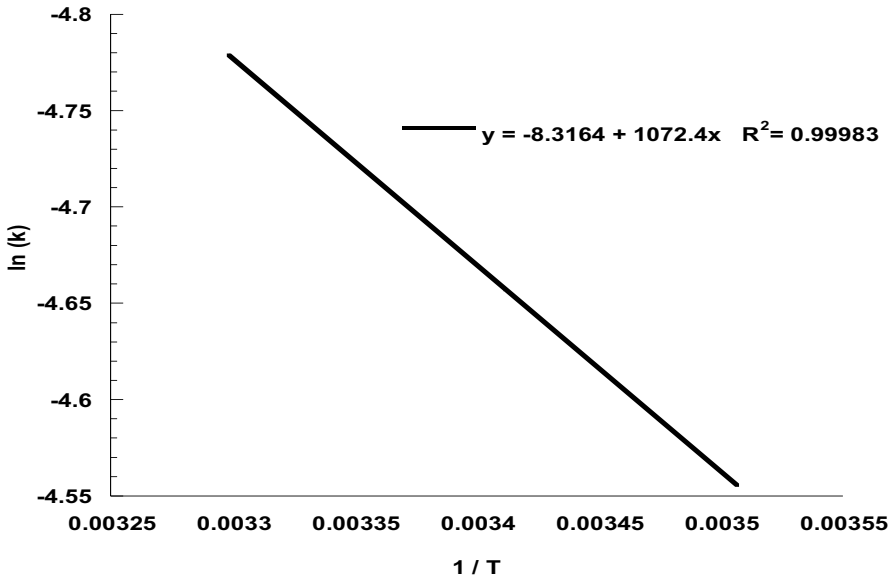

Figure 11: Arrhenius plot for the degradation of SIM by the 20 mmol ZnO/GO photocatalyst

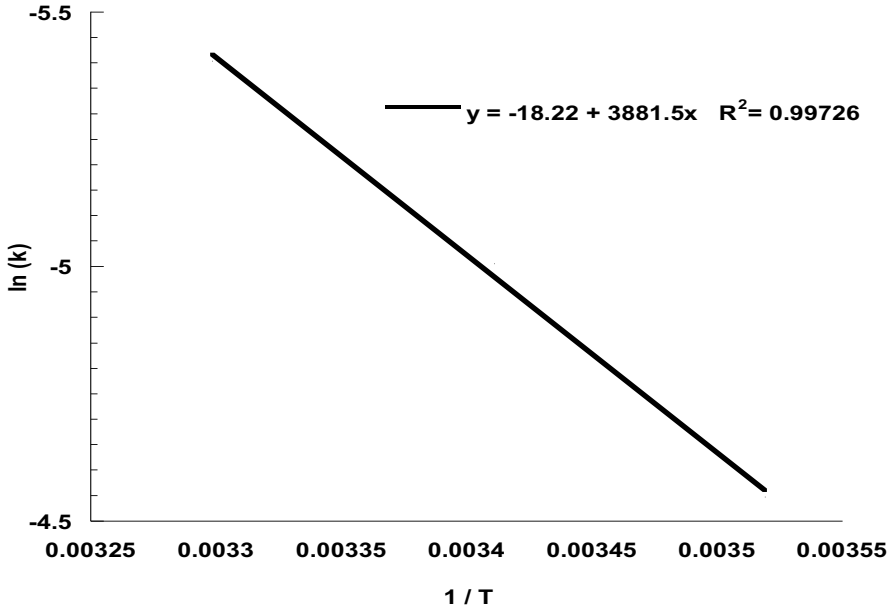

Figure 12: Arrhenius plot for the degradation of SIM by the 10 mmol ZnO/GO photocatalyst

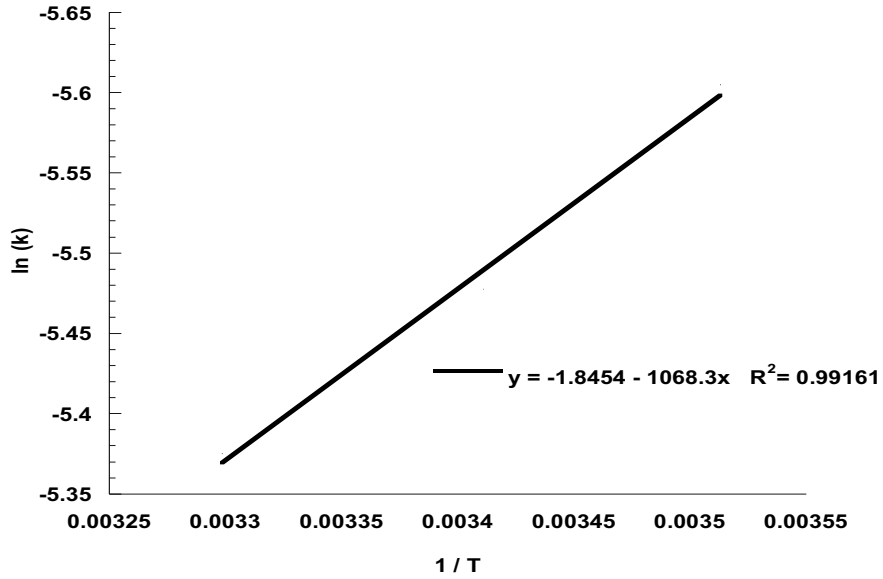

Figure 13: Arrhenius plot for the degradation of SIM by the pure ZnO photocatalyst

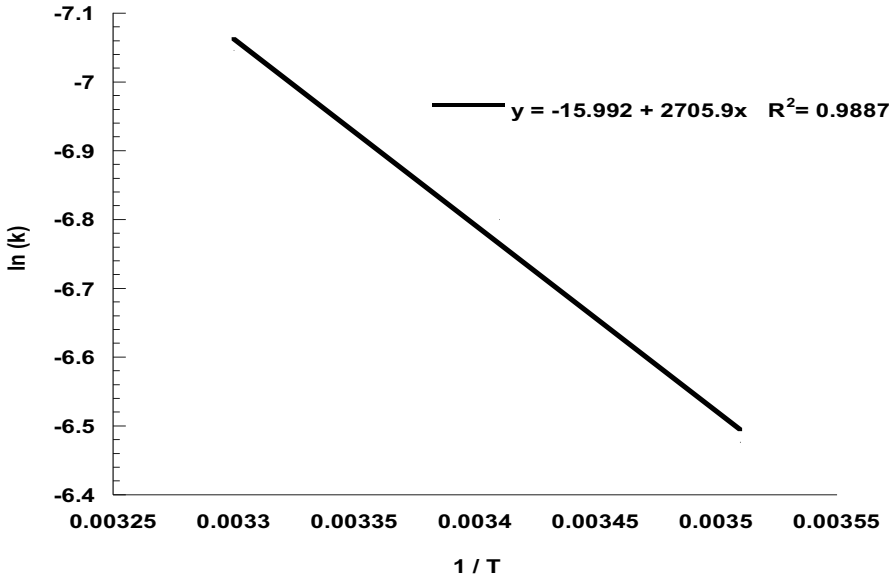

Figure 14: Arrhenius plot for the degradation of SIM by direct photolysis

Photocatalyst	Activation Energy
30mmol ZnO/GO	34.054 kJ/mol
20mmol ZnO/GO	-8.915 kJ/mol
10mmol ZnO/GO	-32.275 kJ/mol
ZnO	8.882 kJ/mol
Direct Photolysis	-22.028 kJ/mol

Table 4: Activation energies associated with the degradation of SIM by ZnO/GO (30,20,10mmol), pure ZnO, and direct photolysis

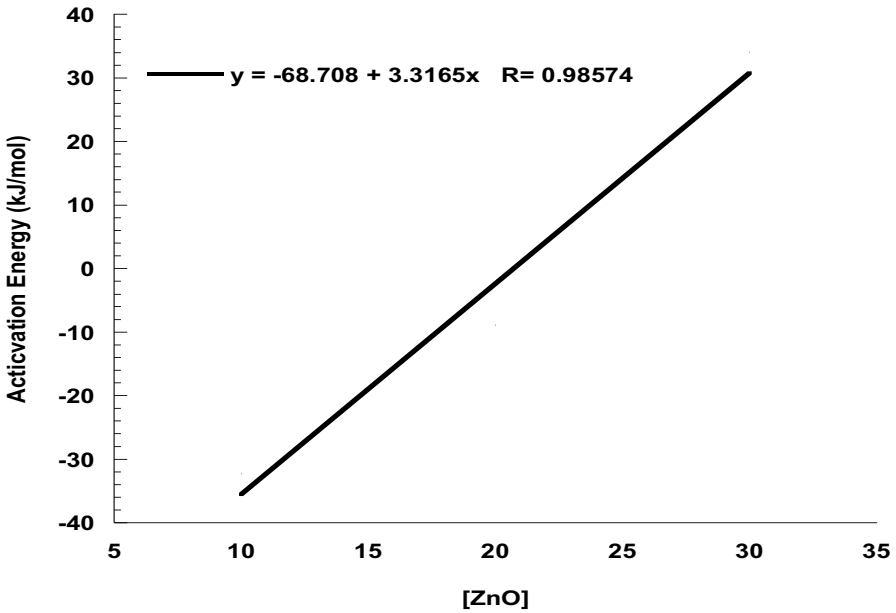

Figure 15: Variance in Activation Energies as a function of ZnO concentration

Arrhenius plots for the process of SIM degradation by ZnO/GO (30, 20, 10mmol), pure ZnO, and direct photolysis are shown in figures 10 – 14. The slopes of these Arrhenius plots were utilized to calculate the activation energies of each process and the corresponding values displayed in Table 4. SIM degradation by the 20 & 10mmol ZnO/GO catalyst, as well as direct photolysis, proceeded in an exothermic nature with higher rates of degradation observed at lower temperatures. The 30 mmol and pure ZnO catalyst acted in the inverse, with a temperature correlation of an endothermic reaction.

Reporting an endothermic reaction for the 30mmol catalyst, and an exothermic reaction for the 20 & 10mmol catalyst seems to be a contradictory. The data presented in figure 15. shows the correlation of activation energy vs ZnO concentration, for all ZnO/GO photocatalysts. A correlation coefficient (r^2) of approximately 0.99, indicates a direct relationship between ZnO concentration on GO, and activation energy. A possible reason for this trend, would be competition between SIM and GO interactions with ROS. Considering that the

hydroxyl radical, the driving force of photocatalytic degradation, has a non-selective reactivity; it could be possible that ROS species could be reacting with the exposed portions of GO in the photocatalyst of lower ZnO concentrations (10, 20mmol)[45]. The higher the concentration of ZnO present on the catalyst, the less exposed GO available to compete with SIM for interactions with the ROS. When the reaction temperature is increased the associated kinetic energy of the particles increases comparatively[46]. This effect could be occurring with the 20 & 10 mmol photocatalyst. Therefor the degradation process of SIM, by the 30mmol ZnO/GO photocatalyst, increases proportionally with temperature because there is less competition for ROS interactions during heightened reaction temperatures.

Cycling Studies Results

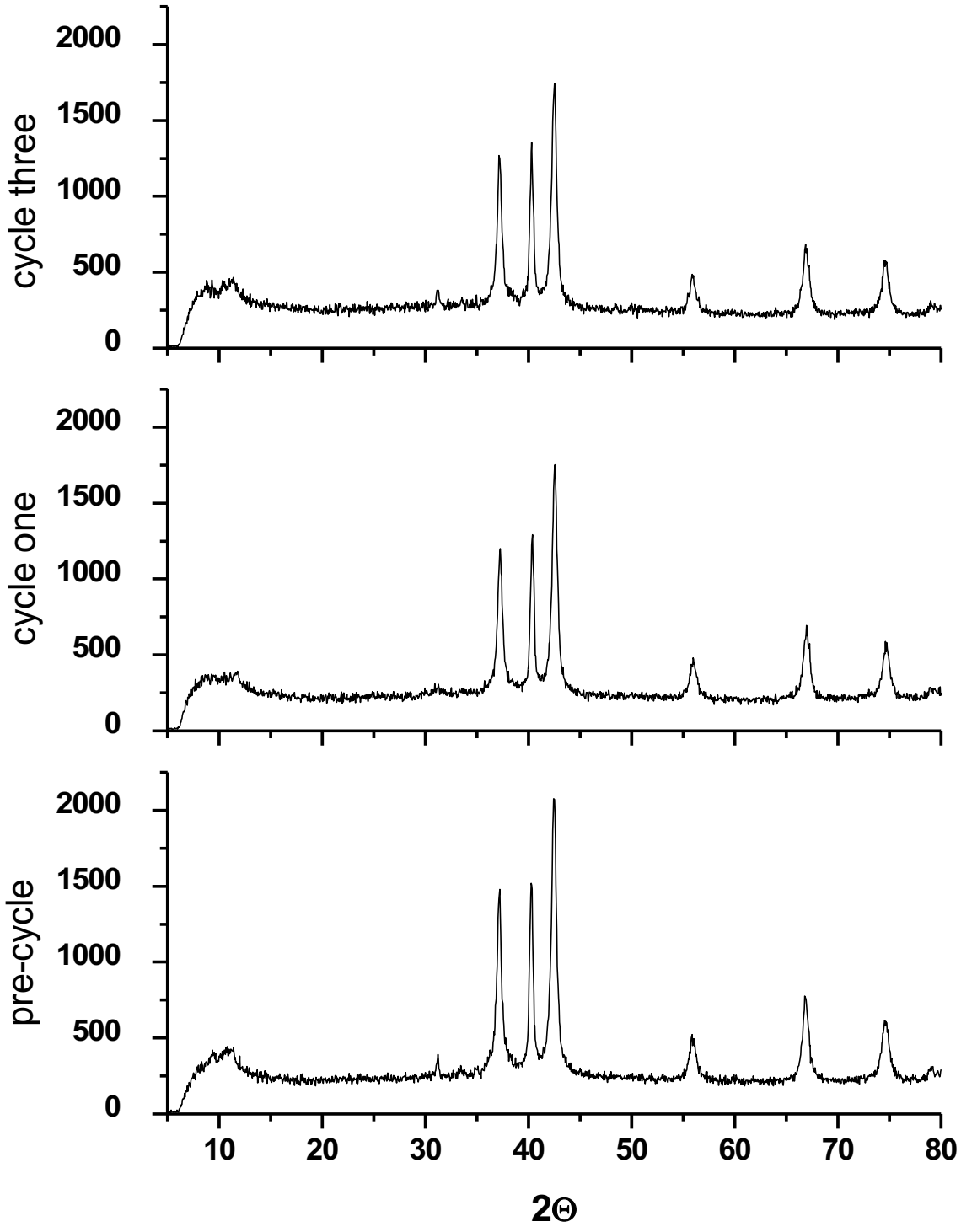

Figure 16: Diffractograms for the XRD analysis of 30mmol ZnO/GO before cycling, after one cycle, and after three catalytic cycles

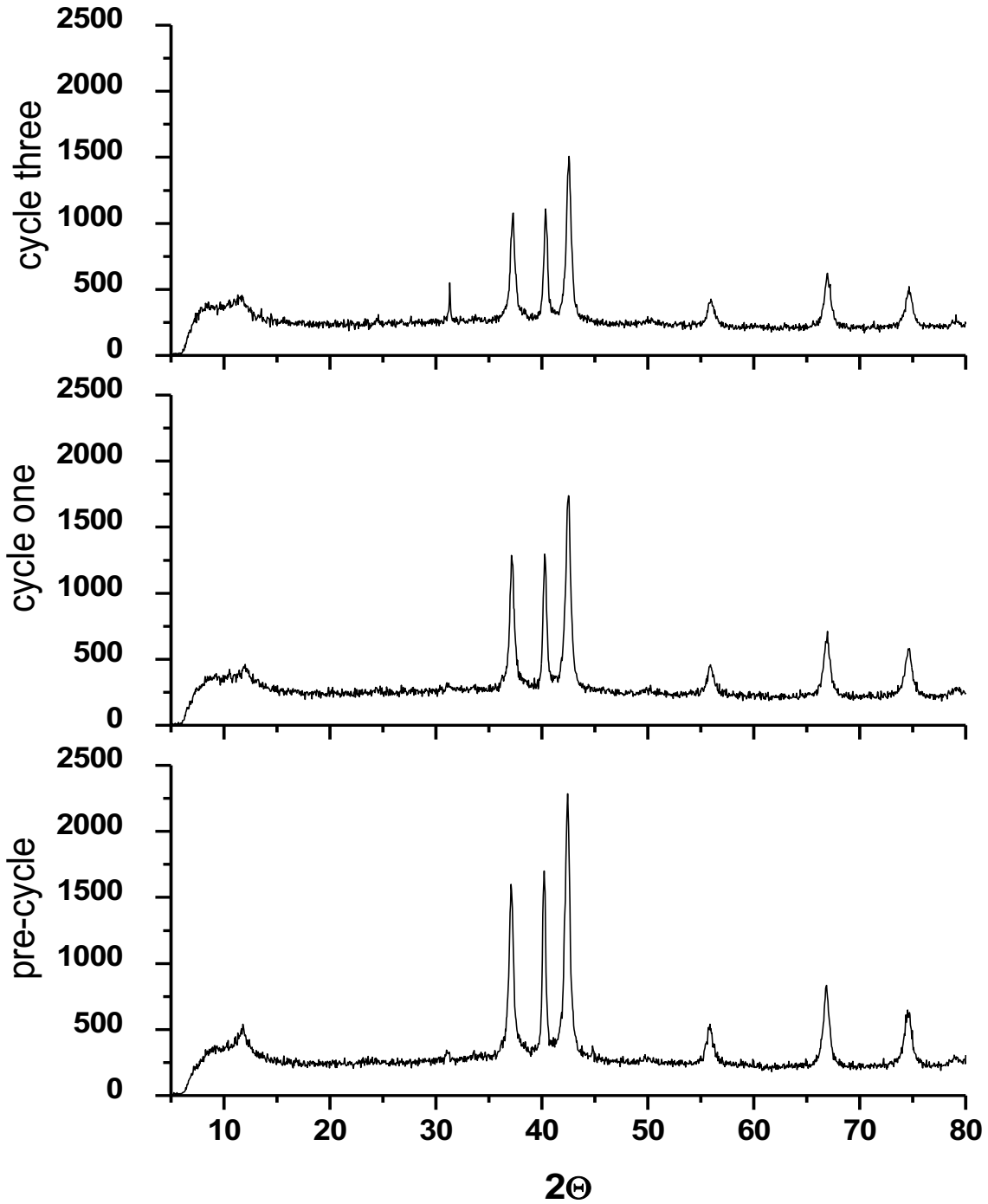

Figure 17: Diffractograms for the XRD analysis of 20mmol ZnO/GO before cycling, after one cycle, and after three catalytic cycles

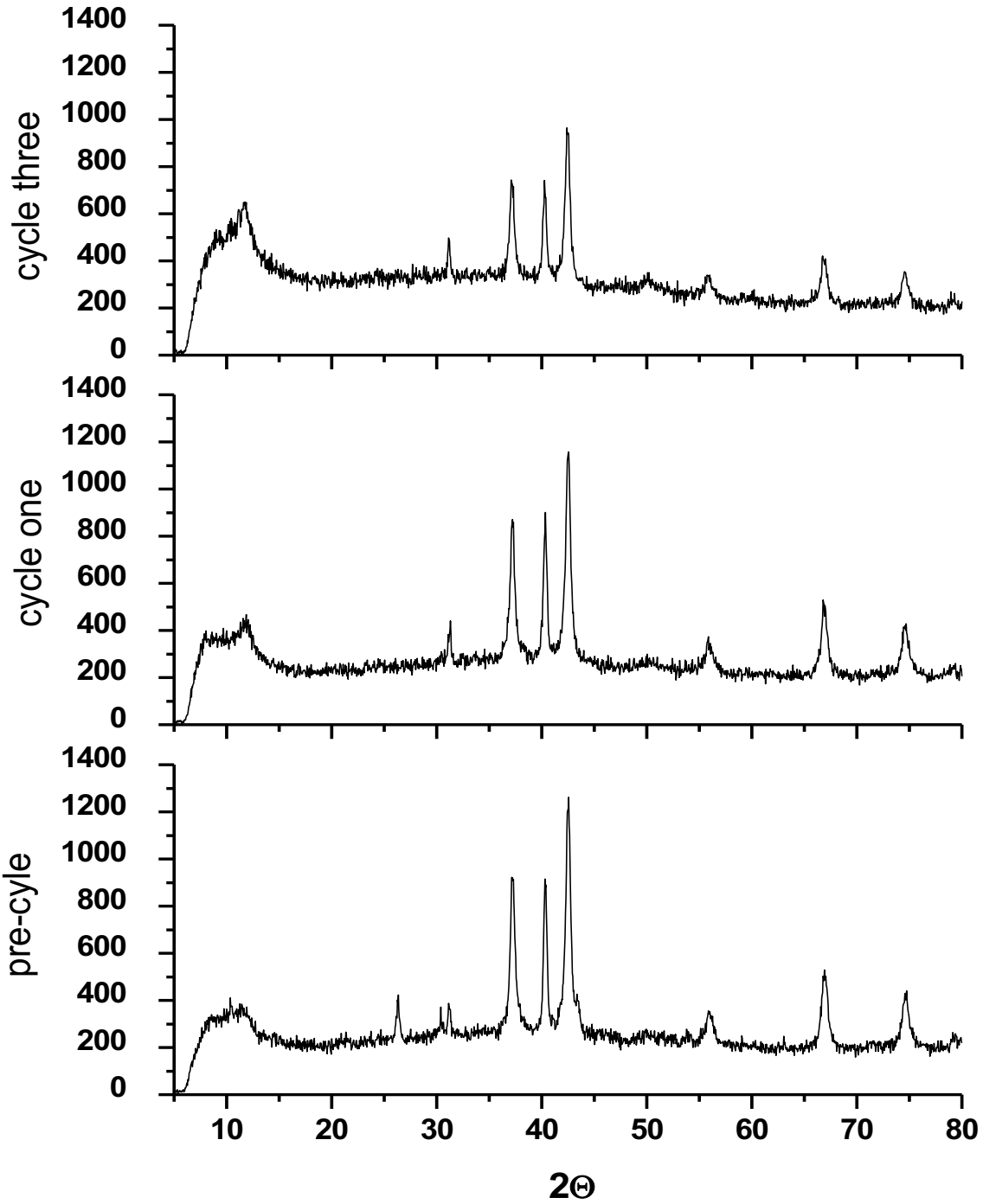

Figure 18: Diffractograms for the XRD analysis of 10mmol ZnO/GO before cycling, after one cycle, and after three catalytic cycles

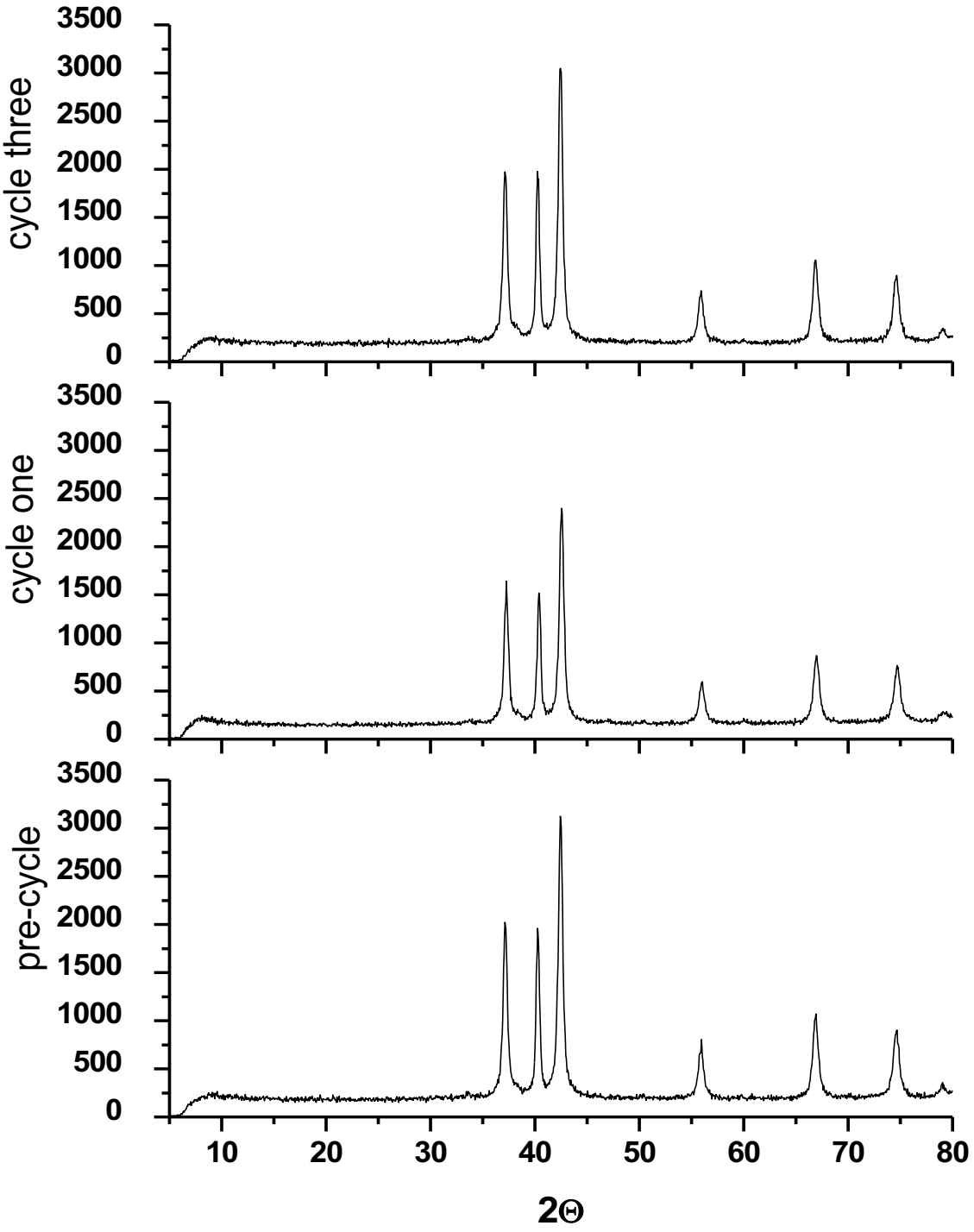

Figure 19: Diffractograms for the XRD analysis of ZnO before cycling, after one cycle, and after three catalytic cycles

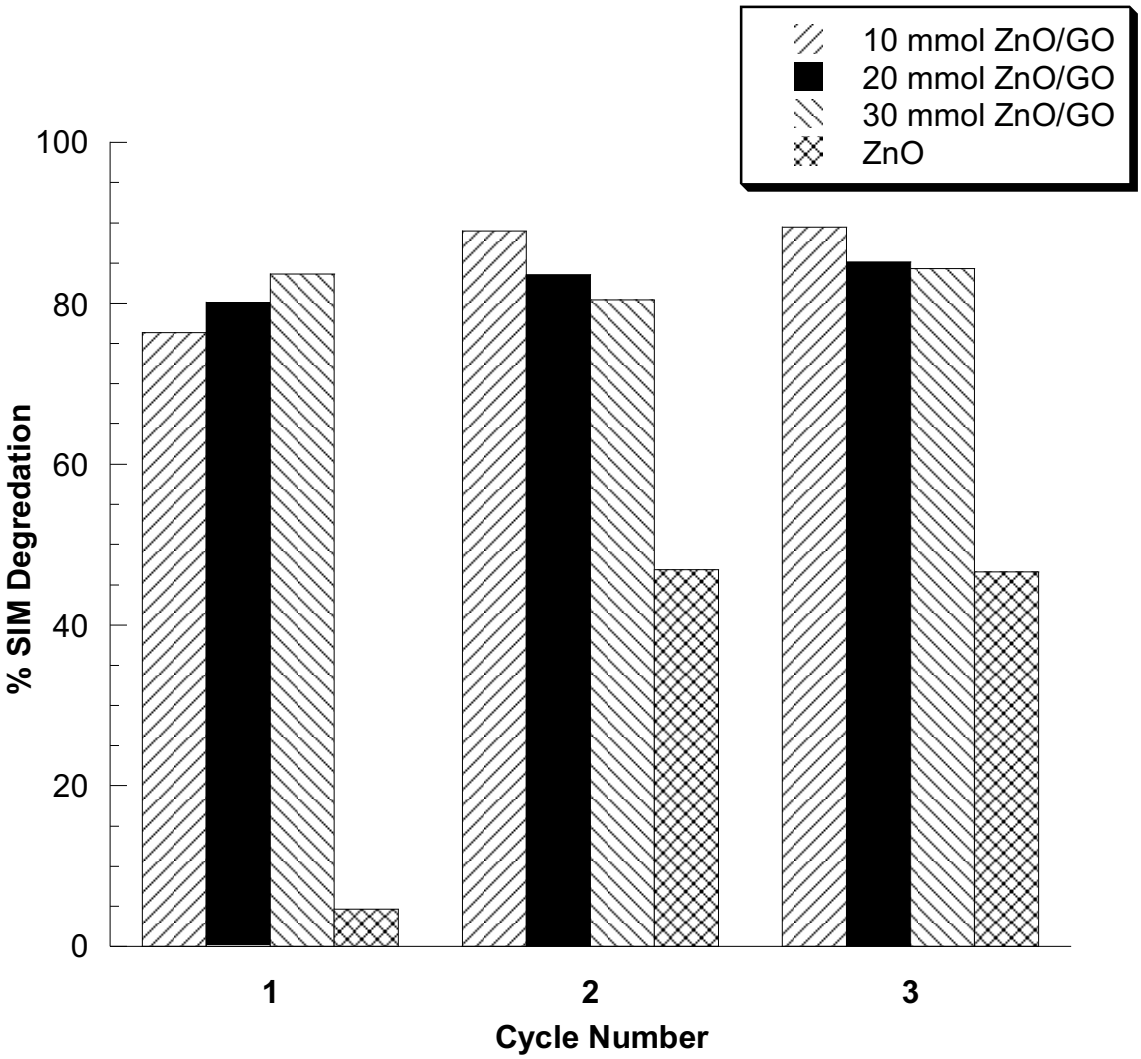

Figure 20: Percent SIM degradation vs cycle number for ZnO/GO (30, 20, 10mmol) and ZnO catalyst

Photocatalyst	Particle size C0	Particle Size C1	Particle Size C2	Particle Size C3
ZnO	22.854nm	23.024nm	23.520nm	23.125nm
10mmol ZnO/GO	22.471nm	21.939nm	21.612nm	21.639nm
20mmol ZnO/GO	22.547nm	22.003nm	21.586nm	22.497nm
30mmol ZnO/GO	21.492nm	20.451nm	20.793nm	20.987nm

Table 5: Particle size of the photocatalyst materials, in nanometers, before catalysis (C0) after one catalytic cycle (C1), after 2 catalytic cycles (C2), and after three catalytic cycles (C3)

All photocatalyst were subjected to three catalytic cycles, in order monitor catalyst efficiency in terms of % SIM degradation. An XRD analysis was performed on each catalyst before and after the 1st cycle, as well as after the 2nd & 3rd cycle in order to observe any possible changes in crystal structure, shown in Figures 16-19. Figure 20 displays the % SIM removed after 1, 2, and 3 catalytic cycles for all ZnO/GO (30, 20, 10mmol) and ZnO photocatalyst. The 20 and 10mmol ZnO/GO composites experienced an increase in photocatalytic efficiency as the number of cycles increased. The 10mmol observed a 13.1% increase while the 20mmol showed an increase of 5.1%, after three cycle lengths. The 30mmol composite maintained nearly the same % SIM degradation throughout the duration of all three cycles. Figure 17 and 18 display the diffractograms from XRD analysis for the 20 & 10mmol composites. Both materials experienced a decrease in intensities for peak located at 37°, 40°, 42.5° in 2θ, for reflections of the (100), (002), (101) planes of hexagonal ZnO at the composites surface. The diffractograms for the 10mmol composite displayed a minor increase in intensity for the peak at 11°, associated with the (002) plane of GO. Each cycle length may reduce the amount of ZnO on the 10mmol surface, therefor exposing the GO support. The intensities of the diffraction peaks in the 30

mmol composite appear to maintain intensity throughout the three cycles; however, minor reductions of intensity can be observed in figure 16. The ZnO photocatalyst experienced the largest increase in % SIM removed, over the three cycle lengths. From the 1st to 2nd cycle the associated % SIM degradation, by ZnO interaction, increased from 4.631 – 46.87%, and was maintained thereafter. Interestingly enough XRD analysis, displayed in figure 18, revealed a decrease in intensities for peaks located at 37°, 40°, 42.5° for the (100), (002), (101) planes of this structure. Similar trends have been reported for photocatalytic materials, such as TiO_2 in literature, with the explanation of reduced particle size over cycle periods[47]. This reduction in particle size could stem from the morphological stress caused by a combination of light absorption & mechanical stirring of the solid photocatalyst. However, this was not the case for these photocatalytic materials, the particle size during cycling studies is reported in table 5. All materials maintained a similar particle size from pre-cycle to third cycle analysis, except for the 10mmol composite, which experienced a minor reduction is particle size. Therefor ZnO, in the hexagonal wurtzite form, requires catalyst priming for reasons other than reduced particle size.

Band Gap Results

Photocatalyst Material	Band Gap (eV)
ZnO (wurtzite hexagonal)	3.37 eV
30mmol ZnO/GO	3.28 eV
10mmol ZnO/GO	3.25 eV
20mmol ZnO/GO	3.11 eV

Table 6: Calculated band gap values for ZnO/GO composites, literature value for ZnO in the hexagonal wurtzite structure

The band gaps for all ZnO/GO composites were calculated through data obtained from % Reflectance studies from UV-VIS spectrophotometer analysis. The band gaps reported for the ZnO/GO composites confirmed a slight narrowing of the band gap when compared to pure ZnO in the hexagonal wurtzite form. This mild reduction in electrical potential between valence and conduction band makes for a photocatalyst with a greater excitation potential under visible spectrum irradiation. Considering that all studies were performed under a metal halide lamp as the illumination source, which has a large output in the visible region of the spectrum, this narrowing of the band gap gives reason for the higher degradation ability of the ZnO/GO composite, when compared to pure ZnO. The ability of absorbing lower frequency energy sources has been reported for the anchoring of semiconductor materials to Graphene Oxide[48].

CHAPTER V

CONCLUSIONS

Synthesized ZnO/GO composites, using varying ZnO concentrations, were characterized via X-ray Diffraction analysis and UV-VIS spectrophotometry. The ZnO/GO composites were utilized as photocatalyst for the degradation process of the herbicide simazine, under visible spectra irradiation. ZnO, in the hexagonal wurtzite crystal structure, was tested alongside these hybrid composites to compare kinetic rates, activation energies, and cycling efficiencies.

To maximize degradation efficiency parameters of initial pH, of SIM solution, and loading mass of the photocatalyst materials were investigated. An initial pH of 2 proved to be most effective for all photocatalysts, in addition, SIM is most soluble at this pH in a range from 2 – 8. A loading mass of 40mg was established as optimal for the loading mass of the 30 & 20mmol catalyst as well as ZnO; the 10mmol composite displayed its highest degradation ability at a catalyst loading of 10mg. The process of SIM degradation proceeded through a second order reaction for all ZnO/GO composites, with a second order dependence on the concentration of SIM present in solution. Kinetic rates of SIM degradation proceeded as followed 30mmol ($4.89*10^{-2}$ $L \cdot mol^{-1} \cdot s^{-1}$), 20mmol ($9.5*10^{-3}$ $L \cdot mol^{-1} \cdot s^{-1}$), 10mmol ($6.7*10^{-3}$ $L \cdot mol^{-1} \cdot s^{-1}$), and pure ZnO ($1.11*10^{-3}$ $L \cdot mol^{-1} \cdot s^{-1}$). These experimentally determined values, expressed a higher rate of SIM degradation for all ZnO/GO composites, when compared to the rate of degradation using pure ZnO. Activation energies proceeded by the inverse of what was to expected from reported kinetic rates. An activation energy of 34.054 kJ/mol was expressed for the 30mmol composite, -

8.915 kJ/mol for the 20mmol composite, and -32.275 kJ/mol for the 10mmol composite. Standard correlations of negative activation energies associated to higher kinetic rates was not observed, therefor the trend of kinetic expression and temperature dependence was explored further. Rates of SIM degradation, expressed from temperature variance, established and endothermic reaction for the 30mmol and pure ZnO photocatalyst, while the 20 & 10mmol proceeded by and exothermic nature. The difference in temperature dependence between the 30mmol and lower concentration ZnO/GO catalyst could possible stem from competition between SIM and GO for reactive oxygen species (ROS). The 20mmol and 10mmol composites have a larger exposure to the reactive Graphene Oxide support, therefor at higher temperatures the rate of ROS to SIM interactions decrease. Cycling studies for all ZnO/GO photocatalysts expressed steady to slightly improved degradation ability throughout the duration of three cycle lengths. The ZnO photocatalyst appeared to require a priming cycle before any appreciable amount of SIM was degraded; following the priming cycle the degradation ability of ZnO, was still lower compared to rate of degradation expressed by the ZnO/GO composites. Calculated band gaps for all ZnO/GO composites indicated that these photocatalyst are well suited for photocatalysis under a visible spectrum light source.

The optimization process and investigative studies for the ZnO/GO composites, utilized as photocatalysts, prove that these hybrid materials work at a higher efficiency than pure ZnO under visible spectra irradiation. The attachment of the semiconducting material, ZnO, to a graphene oxide support successfully produced a photocatalyst with high potential for field application.

REFERENCES

1. Pohansih, Richard P. *Sittig's Handbook of Pesticides and Agricultural Chemicals*. William Andrew, 2015.
2. Ware, G. W. The Pesticide Book. 5th ed. Thomson Publications, Fresno, CA. 2000.
3. Wei Chu, Yongfang Rao, W. Y. Hui. "Removal of Simazine in a UV/TiO2 Heterogeneous System." *Journal of Agricultural and Food Chemistry* (2009): 6944 - 6949.
4. Michael Helm, Dan Wixted. "E X T O X N E T." 1993. *Pesticide Management Education Program.* 26 September 2018.
5. Walter Heri, Frank Pfister, Beth Carrol, Thomas Parshley, James B. Neighbors. "Production, Development, and Registration of Triazine Herbicides." (n.d.): 31.
6. WSSA Herbicide Handbook Committee. Herbicide Handbook of the Weed Science Society of America, 6th Ed. WSSA, Champaign, IL. 1989.
7. Hayes, W.J. and E.R. Laws (ed.). 1990. Handbook of Pesticide Toxicology, Vol. 3, Classes of Pesticides. Academic Press, Inc., NY.
8. Meister, R.T. (ed.). 1992. Farm Chemicals Handbook '92. Meister Publishing Company, Willoughby, OH.
9. Sannino, F., Filazzola, M. T., Violante, A., and Gianfreda, L. 1999b. Adsorptiondesorption of simazine on montmorillonite coated by hydroxyl aluminum species. Environ. Sci. Technol. 33: 4221-4225.
10. Celis, R., Cornejo, J., Hermosin, M. C., and Koskinen, W. C. 1997. Sorption-desorption of atrazine and simazine by model soil colloidal components. Soil Sci. Soc. Am. J. 61: 436-443
11. Celis, R., Cornejo, J., Hermosin, M. C., and Koskinen, W. C. 1998. Sorption of atrazine and simazine by model associations of soil collides. Soil Sci. Soc. Am. J. 62: 165- 171.
12. Garcia-Valcarcel, A. I. and Tadeo, J. L. 1999. Influence of soil moisture on sorption and degradation of hexazinon and simazine in soil. J. Agric. Food Chem. 47: 3895-3900.

13. Juan Carlos Colmenares, Rafael Luque. "Heterogeneous photocatalytic nanomaterials: prospects and challenges in selective transformations of biomass-derived compounds." *Royal Society of Chemistry* (2013): 765-778.

14. Andrew Mills, Stephen Le Hunte. "An overview of semiconductor photocatalysis ." *Journal of Photochemistry and photobiology* (1997): 1-35.

15. Mohammad Mansoob Khan, Syed Farooq Adil, Abdullah Al-Mayouf. "Metal Oxides as photocatalyst." *Journal of Saudi Chemical Society* (2015): 462-464.

16. Catherine B. Almquist, Pratim Biswas. "A mechanistic approach to modeling the effect of dissolved oxygen in photo-oxidation reactions on titanium dioxide in aqueous systems." *Chemical Engineering Science* (2001): 3421 - 3430.

17. Huimin Jia, Weiwei He, Wayne G. Wamer, Xiangna Han, Beibei Zhang, Shu Zhang, Zhi Zheng, Yong Xiang, Jun-Jie Yin. "Generation of Reactive Oxygen Species, Electrons/Holes, and Photocatalytic Degradation of Rhodamine B by Photoexcited CdS and Ag2S Micro-Nano Structures." *Journal of Physical Chemistry* (2014): 21447 – 21456.

18. Dubbaka, Sridhar. "Branched Zinc Oxide Nanostructures: Synthesis and photo catalysis study for application in dye sensitized solar cells." (2008).

19. Daniel Moore, Zhong L. Wang. "Growth of anisotropic one-dimensional ZnS nanostructures." *Journal of Material Chemistry* (2006).

20. Rajesh Kumar, O. Al-Dossary, Girish Kumar, Ahmad Umar. "Zinc Oxide Nanostructures for NO2 Gas Sensor Applications: A Review." *Nano - Micro* (2015): 97 - 120.

21. M. A. Behnajady, N. Modirshahla, R. Hamzavi. "Kinetic study on photocatalytic degradation of C.I. Acid Yellow 23 by ZnO photocatalyst." *Journal of Hazardous Materials* (2006): 226 - 232.

22. Kian Mun Lee, Chin Wei Lai, Koh Sing Ngai, Joon Ching Juan. " Recent developments of zinc oxide based photocatalyst in water treatment technology: A review." *Water Research* (2016): 428 - 448.

23. A. Mathkar, D. Tozier, P. Cox, P. Ong, C. Galande, K. Balkrishnan, A. Leela Mohan Reddy, P.M. Ajayan. "Controlled stepwise reduction and band gap manipulation of graphene oxide." *J. Phys. Chem. Lett* (2012): 986 - 991.

24. Tomas Palacios, Allen Hsu, Han Wang. "Applications of graphene devices in RF communications." *IEEE* (2010): 122-128.

25. J. Du, X. Lai, N. Yang, J. Zhai, D. Kisailus, F. Su, D. Wang, L. Jiang. "Hierarchically ordered macro - mesoporous TiO2 - graphene composite films; improved mass transfer, reduced charge combination, and their enhanced photocatalytic activities." *ACS Nano* (2010): 590 - 596.

26. Kamat, P. V. "Graphene-based nanoarchitectures." *Anchoring semiconductor and metal nanoparticles on a two-dimensional carbon support* (2009): 520-527.

27. Luisa M. Pastrana-Martinez, Sergio Morales-Torres, Jose L. Figueiredo, Joaquim L. Faria, Adrian M.T. Silva. "Graphene photocatalyst." *Multifunctional Photocatalytic Materials for Energy*. Woodhead Publishing, 2018. 79 - 101.

28. R. Saravanan, M.M Khan, F. Garcia, J. Qin, V.K Gupta, A. Stephen. "Ce3+ - ion induced visible - light photocatalytic degredation and electrochemical activity of ZnO/CeO2 nano-composite." *Sci Rep 6* (2016).

29. M. R. Hoffmann, T. Martin, W. Choi, D.W. Bahnemann. "Enviromental applications of semiconductor photocatalysis." *Chem. Rev. 95* (1995): 69-96.

30. A.O. Ibhadon, P. Fitzpatrick. "Heterogenous photocatalysis: recent advances and applications, Catalyst 3." *Catalyst 3* (2013): 189 - 218.

31. K. Nakata, A. Fujishima. "TiO2 photocatalysis: design applications." *Photochem Rev 13* (2012): 169 - 189.

32. M.M. Khan, S.F. Adil, A.A. Mayouf. "Metal Oxides as photocatalyst." *J. Saudi Chem. Soc.* (2015): 462 - 464.

33. Y. I. Choi, S. Lee, S.K. Kim, Y.I. Kim, D.W Cho, M.M. Khan, Y. Sohn. "Fabrication of ZnO, ZnS, Ag-ZnS, and Au-ZnS microspheres, CO oxidation and 2-hydroxyterephthalic acid synthesis." *J. Alloys Compd* (2016): 46-56.

34. H. Chen, C.E. Nanayakkara, V. H. Grassian. "Titanium dioxide photocatalyst in atmospheric chemistry ." (2012): 5919 - 5948.

35. A. Fujishima, T.N Rao, D.A Tryk. "Titanium dioxide photocatalyst ." *J Photocehm Photobiol C: Photochem Rev 1* (2000): 1-21.

36. A.O. Ibhadon, P. Fitzpatrick. "Heterogenous photocatalysis: recent advances and applications, Catalyst 3." *Catalyst 3* (2013): 189 - 218.

37. D. Spasiano, R. Marotta, S. Malato, P. Fernandez-Ibanez. "Solar photocatalysis: materials reactors, some commercial, and pre-industrialized applications." *Appl. Catal. B Environ* (2015): 90 - 123.

38. B. Siwach. S. Sharma, D. Mohan. "Structural, optical and morphological properties of ZnO/MWCNTs nanocomposite photoanodes for Dye Sensitized Solar Cells (DSSCs) application." *J. Integr. Sci. Technol* (2017): 1-4.

39. A. Fujishima, K. Honda. "Electrochemical photolysis of water at a semiconductor electrode." *Nature* (1972): 37-38.

40. Samreen Heena Khan, Suriyaprabha R, Bhawana Pathak, M.H. Fulekar. "Photocatalytic degradation of organophosphate pesticides (Chlorpyrifos) using synthesized zinc oxide nanoparticle by membrane filtration reactor under UV irradiation." *Open access text* (2015).

41. Mohammad Rafi, Babak Samiey, Chil-Hung Cheng. "Study of Adsorption Mechanism of Congo Red on Graphene Oxide/PAMAM Nanocomposite." *Materials* (2018): 1-24.

42. Cockcroft, Jeremy Karl. "Whole Pattern Fitting II. LeBail Method." 2006. *Birkbeck University of London.* 29 November 2018.

43. Thomas M. Ward, Jerome B. Weber. "Aqeous Solubility of Alkylamino-s-triazines as a Function of pH and Molecular Structure." *Journal of Agricultural and Food Chemistry* (1968): 959 - 961.

44. Jessie A. Key, David W. Ball. *Introductory Chemistry*. B. C. Open Text Book Project, 2014.

45. Sasho Gligorovski, Rafael Strekowski, Stephen Barbati, David Vione. "Environmental Implications of Hydroxyl Radicals (•OH)." *ACS Publications* (2015): 13051 – 13092.

46. G. R. Delpierre, B. T Sewell. "TEMPERATURE AND MOLECULAR MOTION." 2005. *physchem.* 12 November 2018.

47. Kalpesh Sorathiya, Biswajit Mishra, Abhishek Kalarikkal, Kasala Prabhakar Reddy, Chinnakonda S.Gopinath, Deepa Khushalani. "Enhancement in Rate of Photocatalysis Upon Catalyst Recycling." *Nature* (2016).

48. Shahid Ameer, Iftikhar Hussain Gul. "Influence of Reduced Graphene Oxide on Effective Absorption Bandwidth Shift of Hybrid Absorbers." *PLOS ONE* (2016): 1-9.

BIOGRAPHICAL SKETCH

Kenneth Ray Flores was born in 1993 in Harlingen, Texas. He grew up and attended high school in Weslaco, Texas. Mr. Flores graduated from Weslaco High School in the Spring of 2011. He attended the University of Texas Rio Grande Valley and graduated in 2016 with his bachelors in Chemistry. Kenneth began the master's degree in chemistry in the spring of 2017, while he conducted research, worked as a teaching assistant, and completed graduate courses. Mr. Flores graduated with his M.S. degree in chemistry in December of 2018. Mr. Flores' permanent mailing address is 1130 Moon Lake North Progreso Lakes, TX 78596 & email address flrs_knny@yahoo.com